



# CHORUS

This is the accepted manuscript made available via CHORUS. The article has been published as:

## Temperature study of the giant spin Hall effect in the bulk limit of $\beta$ -W

Wenzhe Chen, Gang Xiao, Qiang Zhang, and Xixiang Zhang

Phys. Rev. B **98**, 134411 — Published 8 October 2018

DOI: [10.1103/PhysRevB.98.134411](https://doi.org/10.1103/PhysRevB.98.134411)

# **A Temperature Study of Giant Spin Hall Effect in Bulk Limit $\beta$ -W**

Wenzhe Chen and Gang Xiao\*

*Department of Physics, Brown University, Providence, RI 02912, USA*

Qiang Zhang and Xixiang Zhang

*Physical Science and Engineering Division, King Abdullah University of Science and  
Technology (KAUST), Thuwal 23955–6900, Saudi Arabia*

## **Abstract**

Giant spin Hall effect (GSHE) in heavy metals can convert charge current into spin current with a high efficiency characterized by spin Hall angle. In this report, we prepare a set of multilayer systems of  $\beta$ -W/CoFeB/MgO/Ta with the different  $\beta$ -W thickness up to 18 nm. Using a DC magneto-transport method and relying on the anomalous Hall effect of CoFeB, we observed a large spin Hall angle of 63.5% in the bulk limit of  $\beta$ -W solid at room temperature and a weak temperature dependence of spin Hall angle. Additionally, we also studied the crystal structure, magnetization, magnetic anisotropy, electrical transport, spin diffusion and interfacial spin current transmission in this exemplary GSHE system over a broad temperature range of 10 to 300 K, which would benefit fundamental studies and potential spintronics applications of  $\beta$ -W.

\*Gang\_Xiao@Brown.edu

## Introduction

Moore's law [1], which has governed semiconductor technology for decades, has been increasingly challenged in recent years. Rather than relying on electron charge currents, spin current based logic and memory devices are recognized as promising candidates for post-CMOS electronics. One effective way to generate spin current is the giant spin Hall effect (GSHE) [2-8], which is capable of converting charge current into spin current with a high efficiency (hence, the adjective 'giant' is used). Spin current is given by  $J_S = \Theta \times J_c$ , where  $J_S$  and  $J_c$  denote spin and charge current, respectively, and  $\Theta$  denotes the conversion efficiency, namely spin Hall angle (SHA) [2,9]. Since the discovery of GSHE, the spintronics research and development community are actively searching for solids with a large SHA [2,4,8,10-15].

The heavy metals or alloys with strong spin-orbit coupling tend to exhibit large SHAs [4,11,16-18]. Among them,  $\beta$ -phase tungsten ( $\beta$ -W) is one of the most promising GSHE solids [2,11,19-21]. While body-centered-cubic structure  $\alpha$ -W with a moderate resistivity of 30~40  $\mu\Omega$ -cm exhibits a much smaller GSHE,  $A15$  structure  $\beta$ -W with a high resistivity of 100~300  $\mu\Omega$ -cm exhibits a larger GSHE [11,14,22]. The SHA of  $\beta$ -W thin films has been reported to be up to 35% ~ 40% [11,14,23]. Incorporating a large concentration of oxygen into W thin film pushes the SHA even higher to about 50% [10]. It remains an interesting question that what the SHA is in thick or bulk  $\beta$ -W solid.

The purpose of this work is to study the GSHE and find out the maximum SHA in the bulk limit of  $\beta$ -W. Using a delicate deposition and annealing process, we are able to maintain the metastable  $\beta$ -phase of W layer in a multilayer structure of  $\beta$ -W/CoFeB/MgO/Ta with the thickness of  $\beta$ -W that is doubled over what has been achieved in earlier studies [11]. After thermal magnetic annealing under the  $z$ -axis field, we manage to achieve a robust perpendicular magnetic anisotropy (PMA) in the ferromagnetic CoFeB. The CoFeB with PMA acts as an anomalous Hall effect (AHE) sensor to probe the spin-transfer torque as a result of the GSHE-induced spin current from the  $\beta$ -W film [5,6]. This method based on direct-current (DC) electrical transport allows us to determine the *lower bound* value of SHA of  $\beta$ -W [15,24,25], since it is assumed that 100% of the spin currents are transmitted into and absorbed by the CoFeB layer across the  $\beta$ -W/CoFeB interface. In reality, the interface spin transmission is less than unity [15,24,25]. Taking the transmission probability into consideration enables us to

determine the true SHA of our  $\beta$ -W samples. The maximum SHA is thus determined to be 65%, which is the largest in an elemental heavy metal and alloys with strong spin-orbit coupling.

### Sample Preparation and Characterization

We use a home-made high vacuum magnetron sputtering system to deposit a set of multilayer samples on thermally oxidized silicon wafers. The base vacuum pressure is about  $2.0 \times 10^{-8}$  Torr. The MgO is deposited using RF power under argon pressure of 1.2 mTorr, and other layers are prepared using DC power under argon pressure of 2.2 mTorr. To maintain the  $\beta$ -W, we use only 3 Watt of DC sputtering power with a low deposition rate of  $\sim 0.2$  Å/s. Another key point to achieve the thick  $\beta$ -W layer is step-by-step growth, i.e. 75s waiting window period after 25 s growth. After deposition, we pattern the multilayer stacks into standard Hall bars ( $20 \mu\text{m} \times 55 \mu\text{m}$ ) using photolithography and argon ion milling. Finally, we anneal the samples at  $280^\circ\text{C}$  for 1 min in a vacuum of  $\sim 1.0 \times 10^{-6}$  Torr under a  $z$ -axis magnetic field of 0.42 T.

All of our samples have a layer sequence of substrate-Si/SiO<sub>2</sub>/ $\beta$ -W( $x$ )/CoFeB(1.0)/MgO(1.6)/Ta(1.0) (numbers represent the layer thickness in units of nanometer). Each sample has a unique  $\beta$ -W layer thickness ( $x$ ) which varies from 12 to 18 nm. If not specified otherwise, our results are represented by a sample with  $x = 15$  nm. Fig. 1(a) is an illustration of the sample structure  $\beta$ -W/CoFeB/MgO and the Hall effect measurement configuration within a Cartesian coordinate system ( $xyz$ ).

To ensure the crystal phase and the quality of W layer, we characterize our samples using x-ray diffraction (XRD), high resolution transmission electron microscopy (HRTEM), and electrical transport measurement. Fig. 1(b) shows a  $\theta$ - $2\theta$  XRD pattern of a representative annealed sample. The diffraction peaks, (200) and (210), confirm the  $\beta$ -W phase with an  $A15$  type crystal structure [19,22]. According to the Bragg's law, the lattice constant of our W film is  $a = 5.082 \pm 0.016$  Å, consistent with the theoretical value 5.050 Å and other published results [19,22]. Fig. 1(c) gives a HRTEM image of the cross-section of a representative annealed sample. As shown in the enlarged image Fig. 1(d), the interplanar distance of the W layer is 2.3 Å, which is consistent with the  $\beta$ -W's (210) plane's interplanar distance  $d_{210} = \frac{a}{\sqrt{2^2+1^2+0^2}} = 2.258$  Å

[20,22]. Magnetron sputtering usually provides us with films in polycrystalline structure. From the XRD pattern, the crystalline domain's mean size  $\tau$  of the  $\beta$ -W layer is given by Scherrer equation [19,26]:  $\tau = \frac{K\lambda}{FWHM \times \sin\theta}$ , where  $K$  is a dimensionless shape factor (typically  $K = 0.94$ ),  $\lambda$  is the x-ray wavelength, FWHM is the full width at half maximum and  $\theta$  is the Bragg angle. We estimate that the crystalline domain's mean size  $\tau$ , or grain size  $G$ , is  $7.9 \pm 0.8$  nm, which is about half of the W thickness.

The resistivity of 15 nm-thick W film is  $194.5 \mu\Omega\text{-cm}$  at 300 K according to the parallel resistance rule:  $R_{tot} = \frac{R_{\beta-W} * R_{CoFeB}}{R_{\beta-W} + R_{CoFeB}}$  and  $\rho_{\beta-W} = R_{\beta-W} \frac{wt}{l}$ , where  $w$ ,  $t$ ,  $l$  are the width, thickness and length of the  $\beta$ -W layer, respectively. Fig. 1(e) shows the resistivity as a function of temperature from 10 K to 300 K. The temperature coefficient of resistivity of  $\beta$ -W is very small in the whole temperature range. The residue resistivity  $\rho_0$  is  $196.4 \mu\Omega\text{-cm}$ , which is only within 1% variation of the resistivity at 300 K. The weak temperature dependence is an indication that the resistivity is mostly due to the extrinsic inelastic scatterings from spin-orbit coupling defects [19,22].

### **Magnetism and Anomalous Hall Effect (AHE) of CoFeB with PMA**

Next, we characterize the magnetic properties of the CoFeB layer using Vibrating Sample Magnetometer (VSM) of Quantum Design PPMS<sup>®</sup>. Fig. 2(a) shows the magnetization ( $M$ ) hysteresis curves within the  $y$ -axis magnetic field of 2 T at 10 K and 300 K. By extrapolating the high field magnetization towards zero field, we extract the spontaneous magnetization  $M_s(T)$  at various temperature, as shown in the inset of Fig. 2(a). For our 1 nm-thick CoFeB film,  $M_s(T)$  exhibits a linear temperature dependence as expected in a two-dimensional ferromagnet, rather than following the Bloch's  $T^{3/2}$ -law of magnon excitations in three dimensional ferromagnets [18,27,28]. It is noted that  $M_s$  is  $1275 \pm 37 \text{ emu/cm}^3$  at 10 K and  $991 \pm 58 \text{ emu/cm}^3$  at 300 K.

We use the AHE of CoFeB as a sensor to detect the magnetization state. Fig. 2(b) displays a series of Hall resistance hysteresis loops from 10 to 300 K under the  $z$ -axis magnetic field. The nearly perfect square-like hysteresis loops reveal a robust PMA in the 1 nm-thick CoFeB sandwiched between the MgO and the  $\beta$ -W layers. Since the AHE is given by  $\rho_{xy} =$

$R_0 H_z + R_s M_z$  [29], the high and low Hall resistance state represent the spin up and spin down of  $M_z$ , respectively. Fig. 2(c) exhibits a linear relationship between Hall resistance and temperature over the entire temperature range of 10 to 300 K. This linearity is mainly due to the linear temperature dependence of  $M_s(T)$ . At 300 K, the anomalous Hall resistivity is  $0.20 \mu\Omega\text{-cm}$ , corresponding to an anomalous Hall angle of  $\sim 0.2\%$ . The inset of Fig. 2(c) shows the Hall resistance versus  $M_s(T)$ . Based on the linear fitting of the curve, the AHE coefficient for the 1 nm-thick CoFeB is  $R_s = 0.15 \mu\Omega\text{-cm/T}$  [30-32].

The sharp changes between these two states provide the nucleation fields of magnetization switching, *i.e.*, the coercive fields ( $H_c$ ). Fig. 2(d) shows  $H_c$  over the entire temperature range of 10 to 300 K.  $H_c$  is  $5.0 \pm 0.2$  mT at 300 K, increasing to  $36 \pm 1$  mT at 10 K. The  $T^{1/2}$ -dependence is consistent with the model of thermally activated nucleation process in magnetic switching [25], *i.e.*,  $H_c(T) = H_0(1 - A T^{1/2})$ , where  $H_0$  is the coercivity at 0 K and  $A$  is a constant related to the activation energy of domain wall motion. From Fig. 2(b),  $H_0$  is determined to be  $39 \pm 2$  mT and  $A$  is  $2.2 \pm 0.2 \text{ K}^{-1/2}$ .

### Spin Hall Angle of $\beta$ -W

We use the macro-spin model to study GSHE and measure SHA [6,18,25]. In this model, as illustrated in Fig. 1(a), an external field  $\mathbf{B}_{ext}$  with a small angle  $\delta$  to the  $y$ -axis causes the perpendicular magnetization vector  $\mathbf{M}$  of CoFeB to rotate from  $\theta = 90^\circ$  ( $z$ -axis) to  $\theta < 90^\circ$ . Through GSHE, a charge current flowing in the  $\beta$ -W layer is converted into a spin current  $J_s$ , which exerts spin-transfer torque on  $\mathbf{M}$  and causes  $\mathbf{M}$  to rotate further. The angular shift  $\theta$  of  $\mathbf{M}$  can be calculated from the AHE according to  $\sin \theta = \frac{R_H(B_{ext})}{R_H(0)}$ , where  $R_H(0)$  and  $R_H(B_{ext})$  are the Hall resistance at zero field and a finite  $\mathbf{B}_{ext}$ , respectively. Fig. 3(a) shows  $\sin \theta$  as a function of  $\mathbf{B}_{ext}$  under -4 mA and 4 mA charge current. In the absence of  $\mathbf{B}_{ext}$ ,  $\sin \theta$  is 1 as  $\mathbf{M}$  is primarily controlled by the PMA. As  $\mathbf{B}_{ext}$  increases,  $\sin \theta$  approaches zero asymptotically as  $\mathbf{M}$  is driven toward the  $x$ - $y$  plane, overcoming the PMA. In general, the direction of  $\mathbf{M}$  is balanced by three torques [6,11,18]: the torque resulting from the PMA ( $\vec{\tau}_{an} = -\vec{m} \times \vec{B}_{an}$ ,  $\vec{B}_{an}$  being the anisotropic “field”), the torque due to the external field ( $\vec{\tau}_{ext} = -\vec{m} \times \vec{B}_{ext}$ ), and the spin-transfer torque from spin current ( $\tau_{ST} = \frac{\hbar J_s}{2eM_s t}$ ,  $e$  being the electron charge,  $M_s$  and  $t$  the

spontaneous magnetization and thickness of CoFeB, respectively). Under the equilibrium condition  $\tau_{total} = \tau_{ST} + \tau_{ext} + \tau_{an} = 0$ , one obtains the following relation:

$$\frac{\hbar J_s}{2eM_s t} + B_{ext} \sin(\theta - \delta) - B_{an} \sin\theta \cos\theta = 0 \quad (1)$$

where  $\delta$  is the small angle ( $\sim 2^\circ$ ) between the external field and the  $y$ -axis, keeping  $M$  in a coherently rotational state. Fig. 3(a) is the experimental realization of Eq. (1). Under a constant charge current but with opposite parities ( $\pm$ ), there are corresponding  $B_{ext+}$  and  $B_{ext-}$  to maintain a constant  $\sin\theta$ . From Eq. (1), one obtains,

$$B_{ext+} - B_{ext-} = \frac{\hbar J_s}{eM_s t \sin(\theta - \delta)} \quad (2)$$

$$B_{ext+} + B_{ext-} = \frac{B_{an} \sin 2\theta}{\sin(\theta - \delta)} \quad (3)$$

Using data in Fig. 3(a), we present in Fig. 3(b) the value of  $(B_{ext+} - B_{ext-})$  as a function of  $1/\sin(\theta - \delta)$  for various charge currents 1-4 mA at 300 K. As expected, straight lines are observed with slopes of  $\frac{\hbar J_s}{eM_s t} = 2\tau_{ST}$ . Fig. 3(c) shows the spin-transfer torque  $\tau_{ST}$  as a function of charge current in various temperatures 10-300 K. Figure 3(d) shows SHA,  $\Theta = \frac{J_s}{J_c}$ , for the 15 nm-thick  $\beta$ -W in the temperature range from 10 K to 300 K. SHA is  $50 \pm 2\%$  at 300 K and  $49 \pm 2\%$  at 10 K. SHA shows weak temperature dependence and the variance of SHA is about 3% within 10 – 300 K. Similarly, we find that the SHA of the 18 nm-thick  $\beta$ -W is  $57 \pm 2\%$  at room temperature, which is the largest observed SHA among similar GSHE systems [2,4,11,16,18].

Previously, SHA data was obtained in  $\beta$ -W thin film with the thickness up to 9 nm [11], beyond which the metastable phase disintegrates. In the current study, we are able to double the critical thickness up to 18 nm for  $\beta$ -W, as shown in Fig. 4. The finite size effect of SHA is characterized by the spin-diffusion length  $\lambda_{sf}$  according to

$$\frac{\theta(t)}{\theta(\infty)} = 1 - \text{sech}\left(\frac{t_{\beta-W}}{\lambda_{sf}}\right) \quad (4)$$

where  $\theta(\infty)$  is the SHA in the bulk solid [11,33]. Combining the current and earlier SHA results on the  $\beta$ -W/CoFeB/MgO/Ta system [11], we obtain the spin Hall angle  $\theta(\infty) = 56 \pm 3\%$  and the spin diffusion length  $\lambda_{sf} = 4.9 \pm 0.3$  nm in bulk-limit  $\beta$ -W solid.

In the context of other length scales, noting that the effective electron mean free length  $\lambda_{eff} = 0.45$  nm [19], the crystal grain size  $G = 7.93$  nm, and the  $\beta$ -W thickness  $t = 18$  nm, a comparison is observed:  $t > G > \lambda_{sf} \gg \lambda_{eff}$ . It is concluded that the finite layer thickness and the crystal grain size are not the key constraints on the spin diffusion length and the electron mean free length. The spin diffusion length  $\lambda_{sf}$  is about ten times larger than the mean free length  $\lambda_{eff}$ , indicating that the electron spin flips after an average of 11 elastic scatterings.

### Interfacial Spin Current Transmission and Real Spin Hall Angle

In the above analysis, we have assumed the transmission of spin current is 100% at the  $\beta$ -W/CoFeB interface. In reality, the interfacial transparency is less than unity. The loss in transmission is partly due to the spin backflow at the abrupt interface, and partly caused by the enhanced spin scattering from the interfacial region [15,25,34,35]. A semi-classical drift-diffusion formalism has been developed to calculate the spin transmission probability  $P_{tran}$  for the  $\beta$ -W/Ferromagnet (FM) bilayer system [15,21,24,25],

$$P_{tran} = Re \left[ \frac{2G^{\uparrow\downarrow} \tanh\left(\frac{t_{\beta-W}}{2\lambda_{sf}}\right)}{G_{\beta-W} + 2G^{\uparrow\downarrow} \coth\left(\frac{t_{\beta-W}}{2\lambda_{sf}}\right)} \right] \quad (5)$$

where  $G_{\beta-W}$ , is the spin conductance of  $\beta$ -W defined as  $\frac{1}{\lambda_{sf} * \rho_{\beta-W}}$ ,  $G^{\uparrow\downarrow}$  is the spin-mixing conductance of the  $\beta$ -W/CoFeB interface,  $t_{\beta-W}$  is the thickness of  $\beta$ -W and  $\lambda_{sf}$  is the spin diffusion length measured as  $4.9 \pm 0.3$  nm. It has been reported that the real part of the spin mixing conductance of the  $\beta$ -W/CoFeB interface is  $(3.9 \pm 0.8) \times 10^{14} \Omega^{-1}m^{-2}$  [21]. Using Eq. (5), we calculate that  $P_{tran} = 88.1\%$  for our thickest  $\beta$ -W sample (18 nm). Earlier published studies have shown that  $P_{tran}$  ranges from 34 to 67% in Pt/FM systems [15]. The  $\beta$ -W/CoFeB system has a much higher interfacial spin transmission probability due to the higher value of



$\frac{G^{\uparrow}}{G_{\beta-W}}$ . After taking  $P_{tran}$  into consideration, we determine that the real SHA is  $\Theta = 65 \pm 2\%$  for the 18 nm-thick  $\beta$ -W and is  $64 \pm 3\%$  for the bulk limit at 300 K.

### Magnetic Anisotropic Properties of CoFeB

Fig. 5(a) shows the value of  $(B_{ext+} + B_{ext-})$  as a linear function of  $\frac{\sin 2\theta}{\sin(\theta-\delta)}$  at various temperatures 10-300 K. According to Eq. (3), the slopes of the straight lines provide the values of the anisotropy field  $B_{an}(T)$ , which are presented in Fig. 5(b).  $B_{an}(T)$  increases from 537 mT at 300 K to 827 mT at 10 K, which is 22 times larger than the coercive field  $H_c = 37$  mT at 10 K (see Fig. 2(a)). This provides further evidence that the magnetic square-like hysteresis loops are driven by domain nucleation processes [36].

Using the values of  $B_{an}$ , we determine the magnetic anisotropy energy constant,  $K_{eff} = \frac{1}{2}B_{an}M_S$  within 10 to 300 K in Fig. 5(c).  $K_{eff}$  increases from  $2.7 \times 10^6$  erg/cm<sup>3</sup> at 300 K to  $5.3 \times 10^6$  erg/cm<sup>3</sup> at 10 K.  $K_{eff}$  at 10 K is about two times larger than the one at 300 K. The primary contribution to  $K_{eff}$  is the magnetic surface anisotropy responsible for the PMA in the CoFeB layer. The magnetic surface anisotropy constant [18,37] is given by

$$K_s = t(K_{eff} - K_b + 2\pi M_S^2) \quad (6)$$

where  $K_b$  is the bulk magneto-crystalline anisotropy constant. In the thickness region of about 1 nm,  $K_b$  is much smaller than the other two terms in the parenthesis and can be neglected. Using Eq. (6), we determine  $K_s$  at various temperatures 10-300 K, as shown in Fig. 5(d), specifically  $K_s(300K) = 0.88$  erg/cm<sup>2</sup> and  $K_s(10K) = 1.55$  erg/cm<sup>2</sup> at both ends of the temperate range. The MgO/CoFeB interface, rather than the  $\beta$ -W/CoFeB interface, plays a significant role in the magnetic interfacial anisotropy, since comparable values of  $K_s$  have been reported in multilayer systems that share the same CoFeB/MgO interface, but with different interface, e.g., X/CoFeB/MgO (X=Ta, W, Pt) [15,18,38]. Furthermore, the critical role of MgO in sustaining PMA of CoFeB has been reported [39].

## Conclusion

We have extended the critical thickness of metastable  $\beta$ -phase of W thin films to 18 nm in the multilayer system of  $\beta$ -W/CoFeB/MgO/Ta. The crystal structure of  $\beta$ -W is confirmed using XRD and HRTEM. We have investigated magnetic and magneto-transport properties of this system, and particularly its giant spin Hall effect. Using the macro-spin model, we are able to characterize the GSHE of thick  $\beta$ -W films and determine the bulk-limit spin Hall angle is  $56 \pm 3\%$ . We observe that the spin Hall angle doesn't depend largely on temperature and the variance within the whole temperature range is only about 3%. By taking into consideration the spin transmission probability of 88.1%, we have uncovered the real spin Hall angle of  $65 \pm 2\%$  for the 18 nm-thick  $\beta$ -W. This is the largest value ever reported among all transitional metals and alloys at room temperature, attesting the superior candidacy of  $\beta$ -W as an efficient source of spin current generation from normal charge current.

## Acknowledgement

The work was supported by National Science Foundation through Grants No. DMR-1307056, King Abdullah University of Science and Technology (KAUST), and Nanoelectronics Research Initiative (NRI) through the Institute for Nanoelectronics Discovery and Exploration (INDEX).

## References

- [1] G. E. Moore, Proceedings of the IEEE **86**, 82 (1998).
- [2] J. Sinova, S. O. Valenzuela, J. Wunderlich, C. H. Back, and T. Jungwirth, Reviews of Modern Physics **87**, 1213 (2015).
- [3] I. Žutić, J. Fabian, and S. D. Sarma, Reviews of modern physics **76**, 323 (2004).
- [4] L. Liu, C. F. Pai, Y. Li, H. W. Tseng, D. C. Ralph, and R. A. Buhrman, Science **336**, 555 (2012).
- [5] I. M. Miron *et al.*, Nature **476**, 189 (2011).
- [6] L. Liu, O. J. Lee, T. J. Gudmundsen, D. C. Ralph, and R. A. Buhrman, Physical review letters **109**, 096602 (2012).
- [7] W. Chen, L. Qian, and G. Xiao, AIP Advances **8**, 055918 (2018).
- [8] W. Chen, L. Qian, and G. Xiao, Scientific Reports **8**, 8144 (2018).
- [9] J. E. Hirsch, Physical Review Letters **83**, 1834 (1999).
- [10] K.-U. Demasius, T. Phung, W. Zhang, B. P. Hughes, S.-H. Yang, A. Kellock, W. Han, A. Pushp, and S. S. Parkin, Nature communications **7**, 10644 (2016).
- [11] Q. Hao and G. Xiao, Physical Review Applied **3**, 034009 (2015).
- [12] Y. Wang, P. Deorani, X. Qiu, J. H. Kwon, and H. Yang, Applied Physics Letters **105**, 152412 (2014).
- [13] W. Zhang, M. B. Jungfleisch, W. Jiang, J. E. Pearson, A. Hoffmann, F. Freimuth, and Y. Mokrousov, Phys Rev Lett **113**, 196602 (2014).
- [14] C.-F. Pai, L. Liu, Y. Li, H. W. Tseng, D. C. Ralph, and R. A. Buhrman, Applied Physics Letters **101**, 122404 (2012).
- [15] C.-F. Pai, Y. Ou, L. H. Vilela-Leão, D. C. Ralph, and R. A. Buhrman, Physical Review B **92**, 064426 (2015).
- [16] L. Liu, R. Buhrman, and D. Ralph, arXiv preprint arXiv:1111.3702 (2011).
- [17] C.-F. Pai, M.-H. Nguyen, C. Belvin, L. H. Vilela-Leão, D. C. Ralph, and R. A. Buhrman, Applied Physics Letters **104**, 082407 (2014).
- [18] Q. Hao and G. Xiao, Physical Review B **91**, 224413 (2015).
- [19] Q. Hao, W. Chen, and G. Xiao, Applied Physics Letters **106**, 182403 (2015).
- [20] J. Liu, T. Ohkubo, S. Mitani, K. Hono, and M. Hayashi, Applied Physics Letters **107**, 232408 (2015).
- [21] S. Cho, S.-h. C. Baek, K.-D. Lee, Y. Jo, and B.-G. Park, Scientific Reports **5**, 14668 (2015).
- [22] P. Petroff, T. Sheng, A. Sinha, G. Rozgonyi, and F. Alexander, Journal of Applied Physics **44**, 2545 (1973).
- [23] S. Mondal, S. Choudhury, N. Jha, A. Ganguly, J. Sinha, and A. Barman, Physical Review B **96**, 054414 (2017).
- [24] Y.-T. Chen, S. Takahashi, H. Nakayama, M. Althammer, S. T. B. Goennenwein, E. Saitoh, and G. E. W. Bauer, Physical Review B **87**, 144411 (2013).
- [25] P. M. Haney, H.-W. Lee, K.-J. Lee, A. Manchon, and M. D. Stiles, Physical Review B **87**, 174411 (2013).
- [26] A. L. Patterson, Physical Review **56**, 978 (1939).
- [27] G. Xiao, C. L. Chien, and M. Natan, Journal of Applied Physics **61**, 4314 (1987).
- [28] J. Kim, J. Sinha, S. Mitani, M. Hayashi, S. Takahashi, S. Maekawa, M. Yamanouchi, and H. Ohno, Physical Review B **89**, 174424 (2014).
- [29] N. Nagaosa, J. Sinova, S. Onoda, A. MacDonald, and N. Ong, Reviews of modern physics **82**, 1539 (2010).
- [30] Q. Hao, W. Chen, S. Wang, and G. Xiao, Journal of Applied Physics **122**, 033901 (2017).
- [31] S. B. Wu, T. Zhu, X. F. Yang, and S. Chen, Journal of Applied Physics **113**, 17C717 (2013).
- [32] T. Zhu, P. Chen, Q. H. Zhang, R. C. Yu, and B. G. Liu, Applied Physics Letters **104**, 202404 (2014).
- [33] L. Liu, T. Moriyama, D. C. Ralph, and R. A. Buhrman, Physical Review Letters **106**, 036601 (2011).

- [34] J. C. Rojas-Sánchez *et al.*, *Physical Review Letters* **112**, 106602 (2014).
- [35] M. Cecot *et al.*, *Scientific Reports* **7**, 968 (2017).
- [36] S. Ikeda *et al.*, *Nat Mater* **9**, 721 (2010).
- [37] M. T. Johnson, P. J. H. Bloemen, F. J. A. d. Broeder, and J. J. d. Vries, *Reports on Progress in Physics* **59**, 1409 (1996).
- [38] T. Zhu, Y. Yang, R. C. Yu, H. Ambaye, V. Lauter, and J. Q. Xiao, *Applied Physics Letters* **100**, 202406 (2012).
- [39] M. Yamanouchi, R. Koizumi, S. Ikeda, H. Sato, K. Mizunuma, K. Miura, H. D. Gan, F. Matsukura, and H. Ohno, *Journal of Applied Physics* **109**, 07C712 (2011).

## Figures and Captions

Fig. 1

a) A schematic view of the sample under transport measurement with y-axis charge current  $J_c$  under the external field  $\vec{B}_{ext}$ .  $\vec{M}$  is the magnetization vector of the CoFeB layer with PMA.

b)  $\theta$ - $2\theta$  X-ray diffraction pattern confirming  $\beta$ -W phase.

c) and d) HRTEM image of the cross-section of the multilayer sample. The atomic interplanar spacing is 2.3 Å.

e) Resistivity of the  $\beta$ -W layer versus temperature.

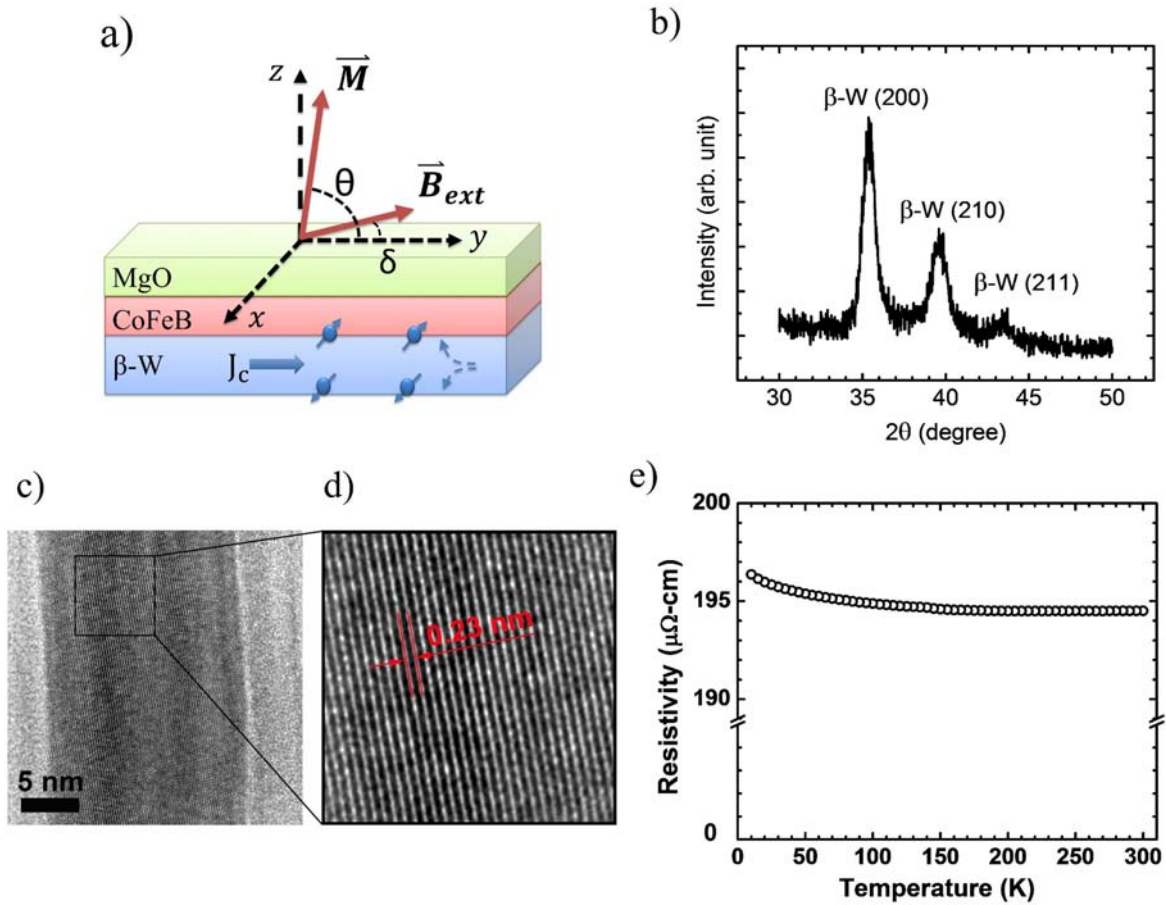


Fig. 2

a) Magnetization hysteresis loops at 10 and 300 K. The inset shows the linear temperature dependence of the spontaneous magnetization of the 1 nm-thick CoFeB layer.

b) Anomalous Hall resistance under a perpendicular magnetic field along the  $z$ -axis in the temperature range from 10 to 300 K. The high and low Hall resistance state correspond to the spin-up and spin-down state of the CoFeB layer, respectively.

c) Hall resistance versus temperature. The inset shows the linear correlation between the Hall resistance and magnetization.

d) The  $T^{1/2}$ -temperature dependence of the coercivity of the CoFeB layer obtained from Fig. 2 b).

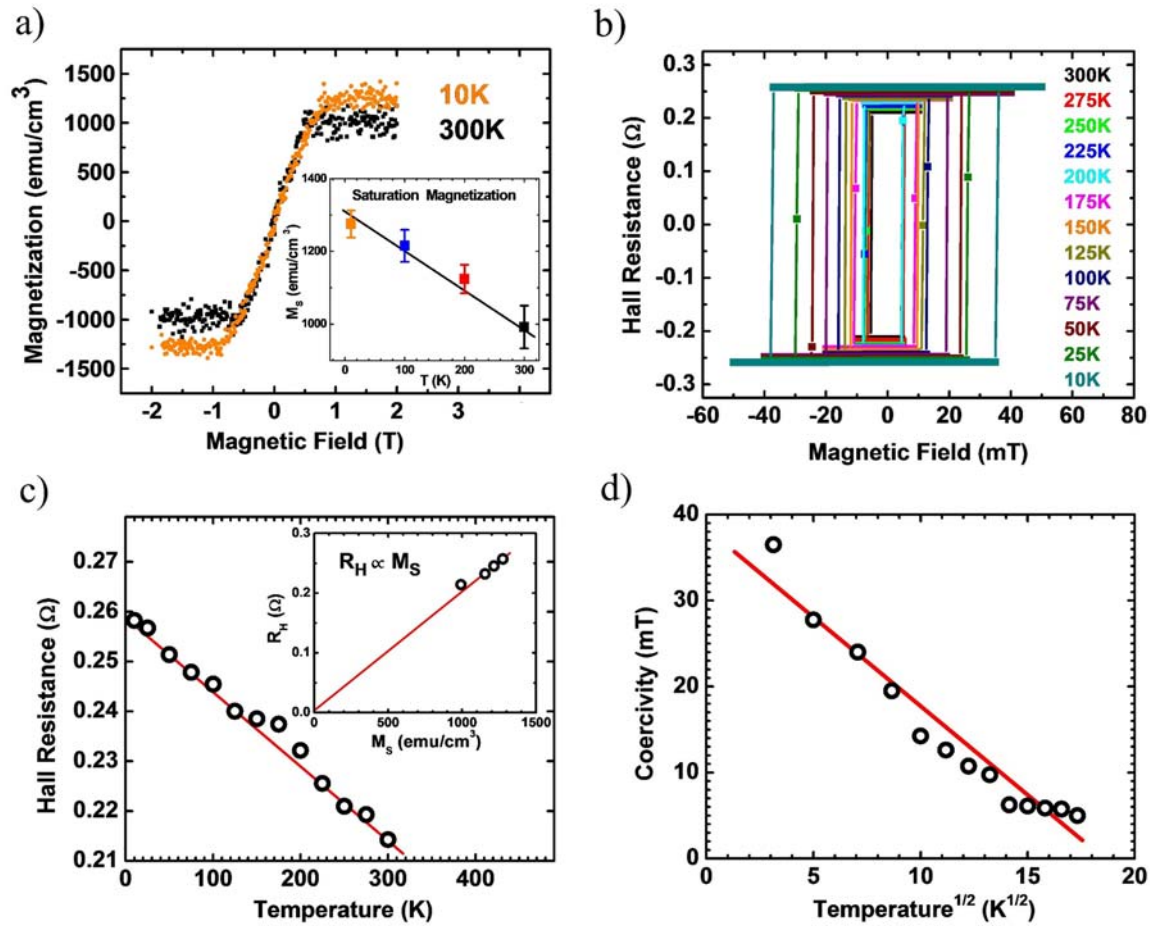


Fig. 3

a) The value of  $\sin\theta$ , determined from the anomalous Hall effect measurement, versus the external field with the charge current of +4 mA (black) and -4 mA (red) at 300 K.  $\theta$  is the angle of magnetization relative to the z-axis. At each specific  $\sin\theta$ ,  $B_{ext+}$  and  $B_{ext-}$  correspond to the positive and negative charge current, respectively.

b) The value of  $B_{ext+} - B_{ext-}$  versus  $1/\sin(\theta - \delta)$  with different charge currents at 300 K.

c) Spin-transfer torque versus charge current at different temperatures.

d) Spin Hall angle of 15 nm thick  $\beta$ -W versus temperature.

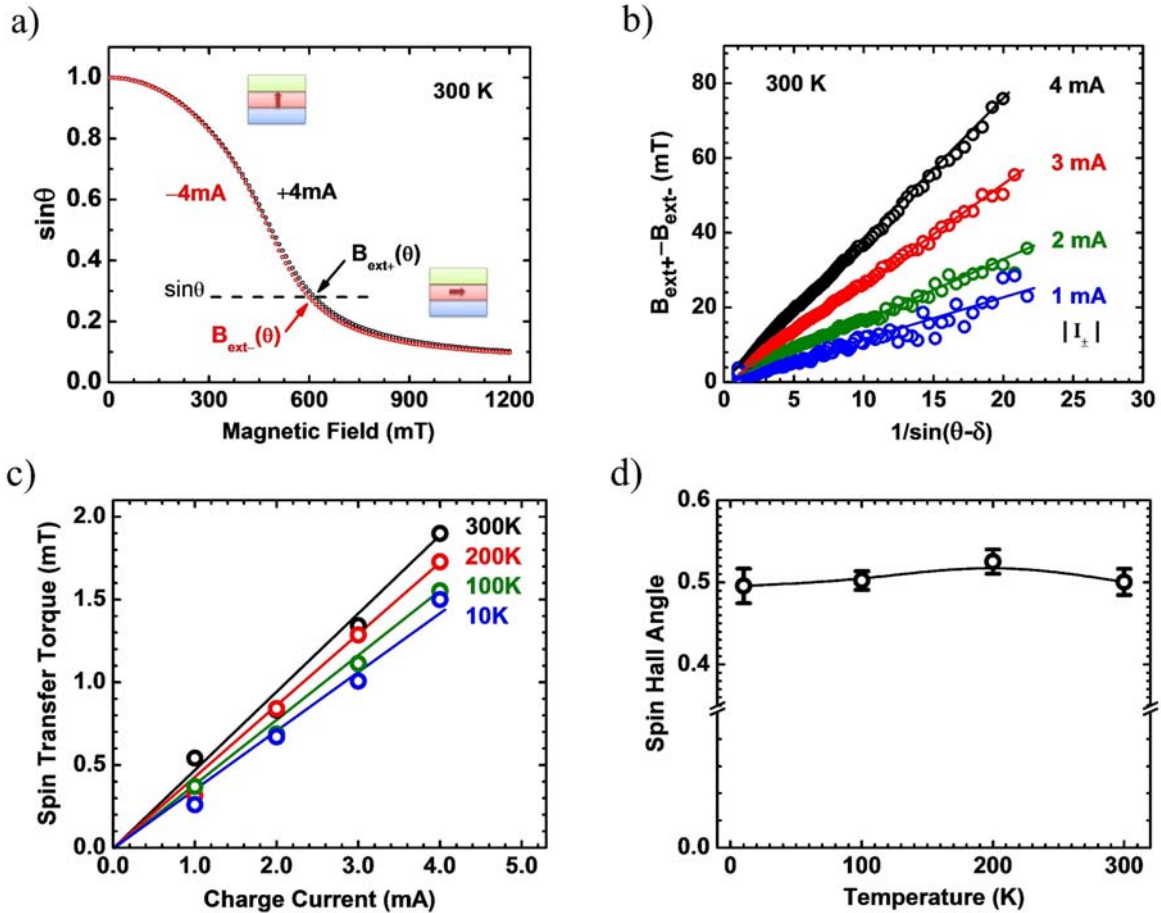


Fig. 4

Spin Hall angle versus  $\beta$ -W thickness, including previous data (green) and current data (black) which has doubled the critical thickness from 9 nm to 18 nm.

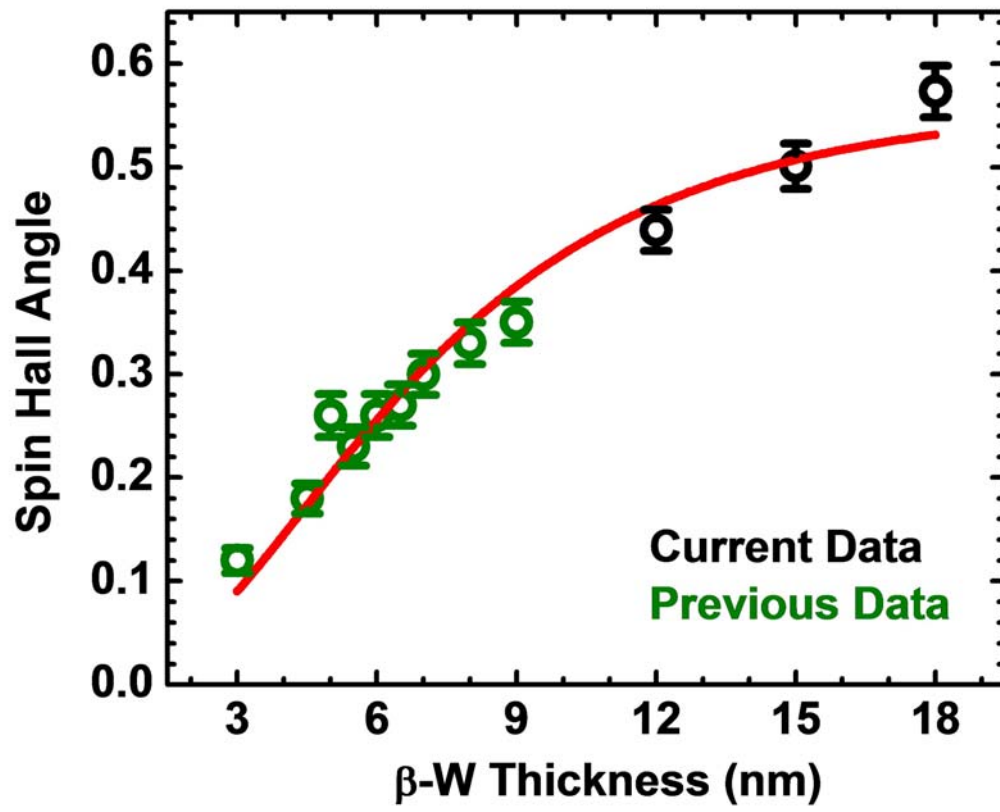




Fig. 5

- The value of  $B_{ext+} + B_{ext-}$  versus the value of  $\frac{\sin 2\theta}{\sin(\theta-\delta)}$  at different temperatures.
- Magnetic anisotropy field  $B_{an}$  versus temperature.
- Magnetic anisotropy constant  $K_{eff}$  versus temperature.
- Magnetic surface anisotropy constant  $K_s$  versus temperature.

